Infrared Avalanche Photodiode Detectors

Anand Singh and Ravinder Pal

Solid State Physics Laboratory, Delhi - 110 054, India
E-mail: ananddhakad@gmail.com

ABSTRACT

This study presents on the design, fabrication and characteristics of HgCdTe mid-wave infrared avalanche photodiode (MWIR APD). The gain of 800 at - 8 V bias is measured in n^+-v-p^+ detector array with pitch size of 30 μm. The gain independent bandwidth of 6 MHz is achieved in the fabricated device. This paper also covers the status of HgCdTe and III-V material based IR-APD technology. These APDs having high internal gain and bandwidth are suitable for the detection of attenuated optical signals such as in the battle field conditions/long range imaging in defence and space applications. It provides a combined solution for both detection and amplification if the detector receives a very weak optical signal. HgCdTe based APDs provide high avalanche gain with low excess noise, high quantum efficiency, low dark current and fast response time.

Keywords: Avalanche photodiode detectors; APD; HgCdTe; Gain-band width product; Excess noise

1. INTRODUCTION

Detection of camouflaged and low temperature/emissivity targets particularly at long range or in the battle field/humid environments become a challenge. If the signal to noise ratio is low, the post detector amplification is also not helpful. Detection and amplification in the photo detector itself is one of the main requirements in such cases. High gain with low noise and wide bandwidth are vital for imaging applications. Avalanche photodiodes perform the functions of detection and amplification for the attenuated optical signals in the battle field and long range applications, especially in space based thermal imaging applications[1-14]. APD provides high internal gain and fast response time, which are needed to meet the system requirements. This paper updates the development on HgCdTe based APDs and also covers other III-V based IRAPDs.

Avalanche photodiode detectors are generally fabricated using $n^+/n^-(v)/p^+$ structures as shown in Fig. 1. Electrons and holes in the depletion region of an APD get accelerated under the influence of a high electric field and gradually acquire sufficient kinetic energy to impact ionize other electron-hole pairs. These newly generated carriers also obtain enough energy from the field in reverse bias and create another electron-hole pairs. This process is known as avalanche multiplication phenomenon. Electric field across the depletion region separates the photo-generated e^--h pairs and thus contributing into the photo current. The n^- region starts acting as a multiplication zone and the surrounding p^+ region is known as the absorption. Internal photocurrent gain takes place through impact ionisation. The multiplication region of APD plays a crucial role to achieve high avalanche gain at low

bias with low noise and high bandwidth[1-3]. In general, APD operates below the break down voltage of the semiconductor and is known as the linear amplifier for the input optical signal, whereas Geiger mode APD works at greater than of the break down voltage. Geiger mode APD has been used to perform photon detection application in the past. However, the recent advances in low noise amplifier design and device fabrication techniques for suppressing APD multiplication noise have led to the development of a new generation of linear mode single photon counting APD (linear SPAD)[5-8]. The high dark current and long dead times limit to the Geiger mode APD based LADAR seekers for detection of the incoming signals. The Linear APD has been more beneficial:

(i) To find the range information from more than one target in a pixel's instantaneous field of view (FOV)
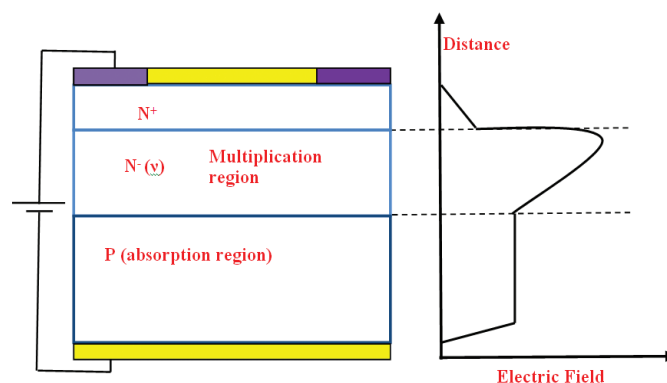

Figure 1. Schematic diagram of an avalanche photodiode illustrating the multiplication process and the absorption region. The electric field distribution is shown in the various regions of the APD diode.

(ii)   To detect the target behind debris with low false alarm rate

(iii) Can employ thresholding technique to reject dark current when they receive reflected signals, and

(iv)   Enable to record the signal intensity that is beneficial to increase in the efficiency[8-10].

In this paper, the significant results of HgCdTe and III-V based APD detector achieved by the leading group are included. The device performance of HgCdTe based APD is simulated as a function of device geometry, material parameters, doping profile, and bandgap profile. High gain and bandwidth, low tunneling and generation-recombination current have been measured. The salient results of our fabricated HgCdTe based APD device are also included. The gain of 800 at -8 V has been measured on HgCdTe based MWIR 320×256 detector array with pitch size of 30 μm. The bandwidth of 6 GHz is estimated in the fabricated device and shows independent behaviour with gain.

2.   III-V MATERIAL BASED IRAPDS

APDs fabricated with Si, InGaAs/InP, InAs, InAlAs (0.3 μm to 1.1 μm), Ge (0.8 μm to 1.6 μm), and InGaAs (0.9 μm to 1.7 μm) show high excess noise at high gain values as both type of carriers participate in the avalanche multiplication process. In the III-V or IV type semiconductors, both electrons and holes contribute in the impact ionisation process due to high multiplication rate. Impact ionisation process is initiated at high reverse bias in these materials. Evacuation rate of charge carriers from the depletion region is also slow[8-12]. High excess noise factor (F) is reported in Si and III-V based materials due to the involvement of both type of carriers (electrons and holes) in the multiplication process. Band width is achieved in the range of 300 GHz - 400 GHz in III-V APDs[10-11]. Several groups are involved in the development of the advanced APD detector for detection of ultraviolet (UV) light signals[14-19]. AlGaN, having direct band gap, is also attractive material for the fabrication of UV APDs[18-19]. It provides a low gain at high reverse bias and low responsivity as compared to other materials[11,14]. Ulmer reported GaN/AlGaN based UV APD (λ_c = below 350 nm) with Q.E. ~ 70 % at 250 nm, responsivity ~ 100 mA/W at reverse bias of 20 V[15]. Yan[18], et al. also demonstrated 4H-SiC based APD for visible band or near visible band UV application with maximum photo responsivity 106 A/W at 370 nm with high reverse bias (> 80 V). Feasibility of fabricating InAs, InSb, InAsSb or InAlSb based APDs have also been reported[20-23]. InAsSb material, having low bandgap and high electron mobility, can be used in low power and high frequency applications for long-wave and mid-wave infrared regions[21]. Abautret et al. reported InSb SAM APD with 1μm thick multiplication layer and doping of less than 1×10^{15} cm^{-3} and achieved the gain ~ 10 at – 5 V and 77 K operating temperature[12]. Low-noise NIR linear mode APD can be used in high-sensitive telecommunications receivers of optical fiber systems and deep space mission[8-10]. Quantum dot based MWIR APD has been demonstrated the peak conversion efficiency of 0.84 per cent and photo current of 0.36 nA at -2 V bias (at 77 K) by Ramirez[24], et al. They also reported high excess noise factor and shows dependent behaviour with the gain. Table 1 summarises the results reported by some groups working on III-V based APD devices.

Table 1.   III-V material based reported APD: The salient features included such as gain, dark current, excess noise, device technology, operating temperature, composition of material and applications

Group/ Reference	Material, composition (x)/cut-off wavelength (λ_c)	Performance	Application
Boeing Spectro Lab[8]	InGaAs/ InP in Geiger mode, λ_c = 1.55 μm	32 × 32 array; V_b > 2 Volt; responsivity~ 100 A/W at 60 V; photon detection efficiency ~ 30%	Demonstration of 3D imaging using LADAR
EPFL[19]	Si ; ultraviolet selective APD; (0.38 μm)	Gain = 50 in UV, and 20 in Visible/near IR ranges; F~ 2.8 at gain of 20.	Selective detection for UV radiation
HRL[40]	InGaAs (near 1.5 μm)	Gain=10; current =200 nA ; 60 micron diameter mesa diodes	Laser range finders/ detection of eye safe laser
Alcatel-Thales[23]	AlInAs on InP substrate for 1.55 μm	I_{dark} = 17 nA; F=3.5; Gain=10; Gain bandwidth product=140 GHz; Responsivity =0.95A/W	Optical telecom-munications
DECE, CHTM[24]	Quantun Dot based (GaAs); λ_c = 3-5 μm	Conversion efficiency = 0.84%; photo current ~ 7.1 $\times 10^{-10}$ A at -2 V; F >>1	----------
SAGEM, SAFRAN[13]	InGaAs (1.5-1.6 μm)	320×256 arrays; pixel pitch =20 μm - 30 μm; Gain <100; dark current < 200 nA/ cm²; Q.E.~ >70-80%	Active imaging in SWIR band
Voxtel[52]	InGaAs/InAlAs for SWIR region (0.95-1.3 μm)	Gain =1000 achieved using linear mode region at 185 K operating temp	High speed photon counting
Sheffield[20]	(i) $In_{0.53}Ga_{0.47}As/ GaAs_{0.51}Sb_{0.49}$ Superlattice for 2.4μm wavelength (ii) InAlAs material for 2.2 μm wavelength	Dark current density ~ 5.5 mA/cm² at room temp., and 70 mA/cm² at 210 K. Gain = 30 at room temp; F~ 2, but not close to unity like HgCdTe at gain of 20.	Optical communication or SWIR active imaging detectors
Sheffield[22]	(i) Ge or Si material for 1.3 to 1.55 μm. (ii) InGaAs on InP substrate for 1.55 μm. (iii) SiC on 4H polytype.	(i) low excess noise achieved rather Si, k value~0.02 and excess noise~2.3 at a gain of 20. (ii) k value~0.1. Gain ~ 10 at 50 V reverse bias.	Telecommunication application.
French[12]	InSb material for 5.2 μm	Gain ~ 10 at V=-4.5 V	--

3. II-VI MATERIAL BASED APDS

HgCdTe is suitable infrared detectors material for niche strategic applications covering 1.3 µm to 16 µm. Asymmetry between effective mass of electron in the conduction band and heavy hole results in the unequal ionisation coefficient for electron and hole in HgCdTe material[25-28]. Electron mobility is two orders of magnitude higher than holes in HgCdTe due to their different scattering rates in HgCdTe. Therefore, the electron penetrates deep into the conduction band prior to interacting with optical phonon, whereas the hole does not acquire sufficient energy. The ionisation threshold energy (E_{th}) for electron and hole is required as approximate equal the band gap ($\sim E_g$) and more than double of E_g, respectively. The ratio of hole and electron ionisation coefficients is near zero i.e. only electron participates in the impact ionisation process owing to the band structure of HgCdTe. For the multiplication process, the charge carriers gain energy from the electric field (ε) under applied reverse bias and lose their energy by scattering (optical-phonons, alloy) or other crystal defects before generating electron-hole pairs. An optical phonon scattering decrease the mean distance covered by the injected first electron and increases the mean ionisation path-length which drops the efficiency of the avalanche phenomenon. At low electric field ($\varepsilon < E_{th}$), the energy achieved by the hot carrier would be lost due to the scattering or impurities and defects. Therefore, hot carrier is unable to initiate the multiplication process. On the other hand, at high electric field, the hot carriers gain sufficient energy ($\sim E_{th}$) from the field faster than they lose it and make possible to the impact ionisation process[28-31]. In HgCdTe material, low phonon scattering also results in the high gain with low noise[27].

Hg$_{1-x}$Cd$_x$Te has a favorable impact ionisation ratio ($k = \alpha_h/\alpha_e$) for different compositions from x = 0.1 to x = 0.7, where α_h and α_e are the ionisation coefficient for hole and electron, respectively. High avalanche gain with low noise is obtained as impact ionisation process is initiated by one type of carriers, electron injection for lower x-values (x < 0.6) or hole injection for[25] 0.6 < x < 0.7. The composition dependence of ionisation coefficient ratio in Hg$_{1-x}$Cd$_x$Te is described as (a) when $\Delta > E_g$, composition $x < 0.6$, and $0 \leq k < 1$; electron is dominant in the multiplication process (Δ=spin-orbit splitting energy), (b) when $\Delta < E_g$, composition $x > 0.7$ and $k \gg 1$; hole is dominant in the multiplication process, (c) when $\Delta \approx E_g$ (at resonance), composition $0.6 < x < 0.7$ and $k \sim 1$; hole is dominant in the multiplication process[25,28]. The excess noise and bandwidth (BW) of APD are determined by α_e and α_h in the multiplication region, which are the characteristics of the material[2].

HgCdTe APDs have been reported in planar and HDVIP structures across the world by several groups including DRS Technologies, CEA-LETI, BAE systems, etc.[32-63]. High avalanche gain ($\sim10^4$) at low reverse bias, low excess noise factor (F~1), high gain bandwidth product (GBW) ~2.1 THz and very short integration time~ 70 ps make HgCdTe APD to be suitable for low optical signal and high speed applications[47,53]. It can be used in the active gated 2D or 3D mode for identification of targets[57]. HgCdTe APD based imaging systems are also being used for eye safe applications in LADAR/LIDAR system[8,9,40]. HgCdTe has fundamental properties and favourable band structure favorable to producing superb detectors for integration in the next generation FPAs. HgCdTe based APD operates at low reverse bias to achieve large internal gain with low excess noise rather than III-V material based APD. Therefore, it is generally preferred linear mode operation to detect the weak signals[11,30-31].

3.1 Performance Parameters of an APD

A photo detector requires high internal gain with low noise and high bandwidth for detection and amplification of attenuated optical signals. A variety of environmental, electrical, and radiometric parameters should be taken into account and carefully controlled. Dark current and the excess noise should be minimised to achieve better performance of APD's[43-44]. High performance of HgCdTe APD has been demonstrated due to the development of advanced device structures and materials.

3.1.1 Excess Noise in the Multiplication Region

In APD, the excess noise is generated by the fluctuation of the photon generated charge carrier. The shot noise (I_S) is described as $I_S = (2\, q\, I\, M^2\, F)^{1/2}$; M = avalanche gain and F= excess noise factor. Figure 2 compiles the dependence of excess noise factor (F) on Gain for different ionisation coefficient ratios $k = \alpha_h/\alpha_e$ in an avalanche photodiode, where electron is dominant in multiplication process. The excess noise factor is constant for $k = 0$ i.e. for pure electron injection but varies with gain[2-3] for $k > 0$.

$$F(M) = M\left[1 + (1-k)\left(\frac{M-1}{M}\right)^2\right] \qquad (1)$$

When hole is dominant in the multiplication process, the F varies with gain for low k-values but constant for $k>50$ i.e. for pure hole injection[2].

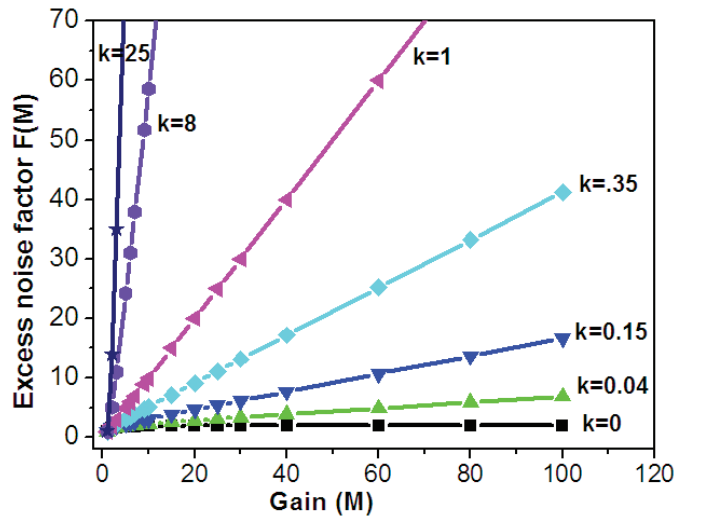$$F(M) = M\left[1 + \left(\frac{1-k}{k}\right)\left(\frac{M-1}{M}\right)^2\right] \qquad (2)$$

Figure 2. The variation of excess noise factor (F) with gain for different ionisation coefficient ratios k = α$_h$/α$_e$ in the APD. F is constant for k = 0 i.e. for pure electron injection (electron is dominant in the multiplication process).

The excess noise in pure electron-injection HgCdTe APD is lower as compared to that of pure hole –injection APD because α_h and α_e are unequal[28-30] for $x < 0.6$. Therefore, HgCdTe e- APD is well suited for low incident flux and active imaging applications from SWIR to LWIR windows.

3.1.2. Dark Current in HgCdTe e-APD

Diffusion, g-r, band to band tunnelling (BTB), and trap assisted tunneling (TAT) currents limit the device performance. But, main concern in e-APD is the minimisation of tunneling current. The contribution of tunneling current affects the device performance at high bias as compared to the diffusion current from p-side of the junction. The doping in v-region is also important because the multiplication process takes place in this region once the electrons reach the multiplication region from the p-region (absorber region). The doping concentration of υ-region is required to low ($< 5 \times 10^{14}$ cm^{-3}) for avoiding the tunneling current contribution at higher bias. If dark current contribution appears into the photocurrent, we can no longer differentiate the avalanche phenomena from the tunneling one[42-44]. Low generation recombination current is also seen in the low bias regime in the APD. Figure 3 shows the dependence of dark current as a function of reverse bias for various doping concentration of υ-region. The dark current density is simulated using the following expression.

TAT current in a uniform electric field depends on the density of the traps and the doping concentration (N)[43].

$$J_{tat} = [10^{-13} N_t V / E_g]$$ (3)

$$\exp\left\{-1.5 \times 10^{10} \pi m_e^{*1/2} E_g^{3/2} / [N(E_g + V)]^{1/2}\right\}$$ (4)

where N_t is mid –band gap states, $m_e^* = 0.07 E_g$ (in eV)

In addition to these currents, BTB current arises due to the electrons from the valence band to the conduction band at high reverse bias[43]

$$J_{btb} = 1.2 \times 10^{-2} V [N(E_g + V)]^{1/2}$$ (5)

$$\exp\left\{-9.43 \times 10^{10} m_e^{*1/2} E_g^{3/2} / [N(E_g + V)]^{1/2}\right\}$$ (6)
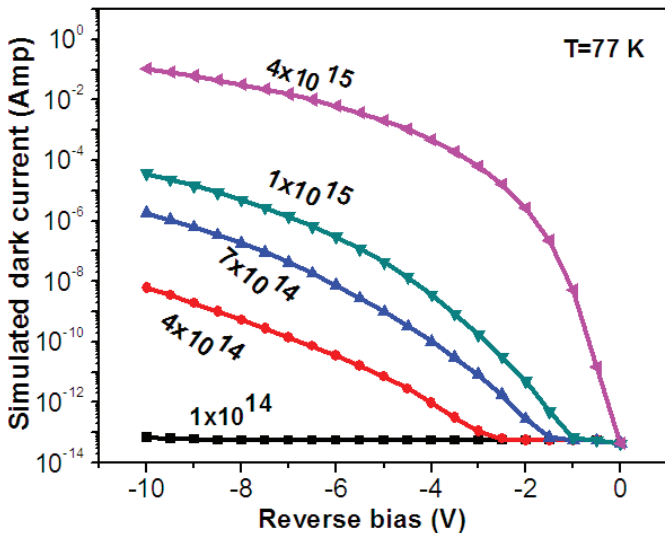

Figure 3. Simulation of dark current as a function of reverse bias for various doping concentration of υ-region in MWIR e-APD.
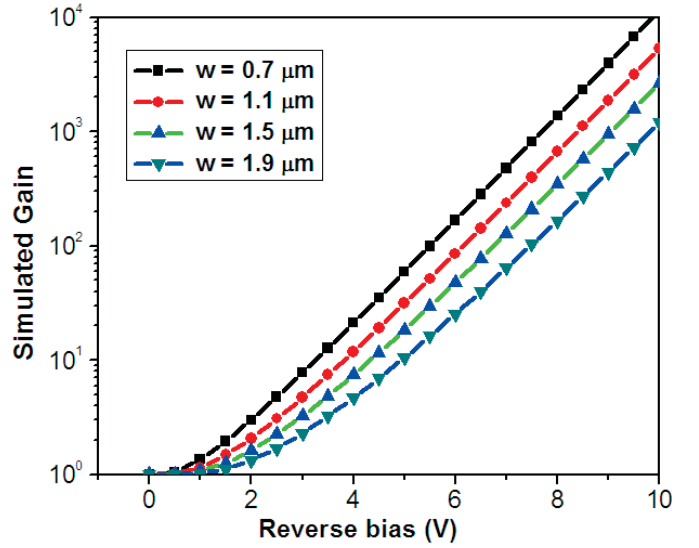

Figure 4. Simulation of gain using Shockley's empirical model for various υ-region width in MWIR e-APDs.

3.1.3 Avalanche Gain

In HgCdTe APDs, only electron involve in the multiplication process ($\alpha_h = 0$); here α_e and α_h are the electron and hole ionisation coefficient, respectively. The avalanche gain (M) is given for depletion width (w) and constant electric field $(E = V/w)$ as[41-42]:

$M = \exp[\alpha(E)w]$, where $\alpha(E) = a E \exp(-b/E)$

Then,

$$M = \exp\left[aV \exp\left(-\frac{bw}{V}\right)\right]$$ (7)

The parameters a and b are defined as $a = q/r E_{op}$, $b = E_{th}/qL_t$, $r = L_t/L_r$, and E_{op} = optical phonon energy. The values are calculated as $a = 1.0741$ V^{-1}, $b = 2.29 \times 10^4$ V/cm in the present study. These values can be adjusted as per device parameters. The above expression is used to study the variation of the gain on set as a function of depletion layer width in MWIR e-APD at 80 K, but parameters a and b are close to independent of depletion width and scaled with band gap. The values of parameters are only applicable at low electric field. Figure 4 represents the simulated gain as a function of depletion region width. The gain is reduced at constant reverse bias with increasing of the multiplication region-width. Hence, larger gain at low bias is obtained in narrow devices, which can be advantageous if the APD can be used with Readout integrated circuits (ROIC) in which the maximum bias can be limited. But, the tunneling current might be contributed in those APD having narrow depletion region[43-44]. Therefore, optimisation of depletion width is very crucial in MWIR e-APD. In order to achieve high gain for e-APD devices, initially the depletion width is small nearly 1.1 μm and corresponds to maximum electric field ∼ 4-5 kV/cm. The multiplication process is started at low reverse bias. The resultant gain increases exponentially with the reverse bias in our fabricated APD device[49,53].

3.2 Development of HgCdTe based APD Device Technology

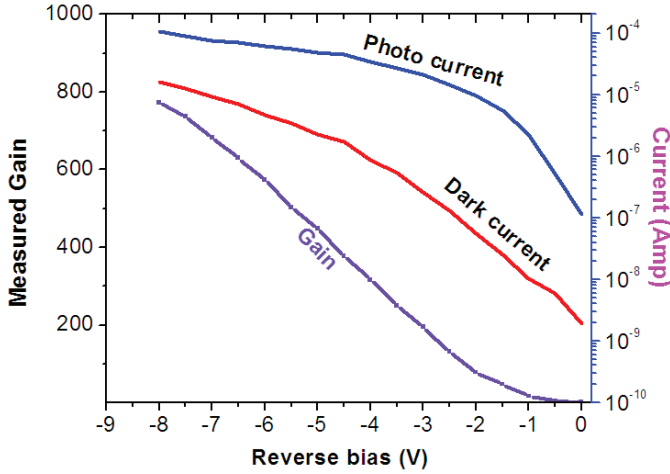In the early stages, HgCdTe APDs were developed in the

Figure 5. Measured dark current, photo current and avalanche gain versus reverse bias for HgCdTe MWIR e-APD at 80 K.

SWIR region for telecommunication applications[32-34]. Shin[32], *et al.* reported the gain ~ 15 at -80 V bias in planar HgCdTe/ CdTe APD (λ_c =1.22 µm). Planar implanted n-on-p photodiode with a gain ~ 5 at -10 V bias and bandwidth ~ 650 MHz were achieved by Alabedra[33-34], *et al.* They demonstrated planar p-i-n $Hg_{0.56}Cd_{0.44}Te$ SWIR APD using electron/hole -injection multiplication processes and reported that (i) electron-injection based APD at low reverse bias provides low excess noise factor as compared to hole injection- APD[34]. Hall[31], *et al.* also reported same results. Impact ionisation in LWIR APD device was first reported by Elliott[35], *et al.*, followed by Vaidyanathan[36], *et al.* reported gain of about 100 (at 3.5 V bias, 77 K) in n^+-n-p planar LWIR e-APD. They have also reported that impact ionisation process was initiated only by electrons. Several groups have been demonstrated that hole-initiated APD devices are suitable for optical fiber transmission systems[31-34].

Beck[26,30], *et al.* pioneered the electron–initiated impact ionisation process in MWIR HgCdTe p-around-n HDVIP photodiode at 77 K temperature and reported the avalanche gain of 50 at normal reverse bias with low excess noise. The gain was uniform from element to element in an array. Kinch[27], *et al.* pioneered a theory, based on the band structure of HgCdTe, for explaining the unequal ionisation process of electron and hole in the avalanche phenomenon. Finally, it is concluded that electron-injection multiplication process is more favorable from SWIR to LWIR APD for achieving high gain at low reverse bias with low noise. Beck[49,61], *et al.* have developed MWIR HgCdTe cylindrical p-around-n e-APD with gain~ 1000 and very low gain normalised dark current density (< 0.7 nA/cm²). However, they reported that the planar APD structure provides fill factor~ 100 % and the collection efficiency > 90%, whereas HDVIP diode has advantage to yields low dark current, high quantum efficiency and high operability.

Reine[38], *et al.* have reported back- illuminated 4 × 4 array of planar MWIR n-on-p e-APDs on LPE grown HgCdTe with acceptor concentration of 2×10¹⁶ cm⁻³. Uniform avalanche gain of 650 with low noise has been shown at -12 V and 160 K temperature.

Rothman[11], *et al.* at CEA/LETI have improved the gain to

5300 (-12.5 V) in planar p-i-n MWIR e-APD (λ_c = 5.0 µm, 77 K) with pixel pitch of 30 µm. They have reported lower dark current, noise factor of 1.0-1.3, and shot noise equivalent input current (I_{eq-in}) = 2.0 × 10⁻¹³ A to 1.0 × 10⁻¹² A under 12 V reverse bias. Perrais[39,47], *et al.* have demonstrated gain of 2800 (-12 V, 77 K, 5.3 µm), RC time constant limited bandwidth ~ 400 MHZ and the GBW = 2.1THz in front-illuminated HgCdTe MWIR e-APD[39,47]. They are first to measure the impulse response time for front side illuminated n-on-p MWIR HgCdTe e-APD at 77 K with λ = 1.55 µm laser pulse[47]. The response time is recorded as the rise time of t_{10-90} = 88 ps and a fall time of t_{90-10} = 2.4 ns. Bandwidth is calculated from the relation, BW = $2.2/2\pi\tau_{response}$. Rothman[59,62], *et al.* of the same group have observed the gain of 600 with excess noise factor (F) =1.2 in short wave e-APD (λ_c= 2.9 µm, x_{cd} = 0.4) at 80 K operating temperature. They have measured gain of 200 with F < 1.3 and dark current = 6.2 µA/cm² with λ_c = < 2.8 µm at 300 K operating temperature. The performance of FPA is enough to enable high sensitivity single element LIDAR application and time of flight imaging[46]. The highest gain for HgCdTe based MWIR e-APD has been reported above 10⁴ at 13.8 V reverse bias by Kerlain[53], *et al.* of the same group. They have demonstrated MWIR APD FPA with 384×288 format and 15 µm pitch for passive amplified and active laser assisted imaging. The performance of FPA has been measured with photon flux at f/2 apertures using black body temperature ranging from 20 °C to 30 °C[57]. Gain operability for best devices achieved 99.74 % at 7 V reverse bias corresponding to gain[53] of 55. A record avalanche gain of 13,000 has been observed on some diodes of APD devices. Borniol[57], *et al.* developed an e-APD 320 × 256 FPA with 30 µm pixel pitch (λ_c = 4.6 µm, operating temp. at 80 K) for active 2D and 3D imaging. The 3D image has been obtained using the LADAR system about 45 meter distance away from the target in which the laser pulse energy is taken about 8 mJ per pulse during 8 ns. The gain of 23 at - 6 V is reported with a laser pulse return energy equivalent to 4300 photoelectrons per pixel.

Mallick[37,51], *et al.* have demonstrated HgCdTe-based MWIR p-i-n APD on Si substrate. They achieved gain of 1250 at -10 V and 410 at -4 V for p^+-n^--n^+ and p^+-n APDs, respectively with excess noise factor ~ 1-1.2. The R_0A of 3 × 10⁶ Ω-cm² and 9 × 10⁵ Ω-cm² are reported at 77 K temperature in these devices[37]. Asbrock[9], *et al.* have demonstrated HgCdTe APD on 4 × 4 arrays with 40 µm pitch and sensor chip assemblies for scanning and starring LADAR systems. The gain above 60 and bandwidth of 1 GHz at 180 K has been reported. Linear mode photon counting has advantages like determination of intensity as well as time of interval and discrimination between optical signals. Therefore, linear operation of APD is utilised in the sensor applications which require low internal gain[6-9,45-46]. Some salient features including the device architecture, fabrication technology, impulse response time, dark current and avalanche gain are shown in Table 2.

3.3 Fabrication and Characteristics of HgCdTe based MWIR e-APD

Vacancy doped p-type $Hg_{1-x}Cd_xTe$ epilayer grown on (111)B CdZnTe substrate with composition x = 0.30, carrier

Table 2. **Gain, noise, bandwidth, operating temperature, pitch size, and impulse response time, device architecture, material parameters, and fabrication technology covering reported results on planar, cylindrical HDVIP and mesa HgCdTe based avalanche photodiodes**

Group	Composition (x)/cut-off wavelength (λ_c)	Device architecture	Device geometry	Performance
French group[33-34]	x = 0.44, λ_c =1.6 to 2.5 µm	p-n⁻-n⁺ junction or planar junction; n⁻- layer is formed by aluminum ion-implantation with (10^{14} cm⁻²; 250 KeV), p-type substrate with doping of 10^{16} cm⁻³	Diameter of active area = 30 µm	BW =1000 MHz at M = 5, Dark Current at -10 V = 2 µA; Sensitivity at 1.3 µm to 2.5 µm » 0.2A/W; Capacitance (at –10 V) < 1pF ; Quantum - efficiency (Q. E.) = 50-60%
Sofradir/ CEA-LETI[11]	λ_c = 5.0 µm	p-i-n junction formed and e-APD; p-type layer with doping~3 ×10^{16} cm⁻³; n⁺ region with doping level of 10^{18} cm⁻³, grown by MBE/LPE.	Pitch size = 30 µm	Gain M= 5300; F=1.0-1.3; I_{eq} in= 2×10^{-13} A to 1×10^{-12} A ; GBW = 723 GHz with maximum gain 5000 at 77 K; rise time t_{10-90}= 88 ps and fall time t_{90-10}= 2.4 ns:
Sofradir/ CEA-LETI[39,44,47]	x = 0.3; λ_c = 5.0 µm - 5.3 µm	p-i-n junction e-APD; doping in p layer : 3 × 10^{16} cm⁻³ ; epitaxial grown by MBE and LPE	Pitch size: 15 µm, and 30 µm;	Gain ~ 5000 at -12 V; F: 1-1.5; first measurement of impulse response time; BW = 600 MHz; GBW=2.1THz at gain of 2800;
Sofradir/ CEA-LETI[59-60,62]	λ_c = 2 µm to 2.9 µm (SWIR)	p-i-n junction e-APD; doping in p layer :1-3 × 10^{16} cm⁻³ ; epitaxial grown by MBE/LPE	320 × 240, pixel pitch: 30 µm; 384 × 288, pixel pitch:15 µm	Gain~ 200; F< 1.3 even at room temp.; operability in FPA >99.5%; Q.E. > 50 %; dark current density~ 6.2 µA/cm² at 200 K; response time measurements using 1.55 µm laser pulse
Sofradir/ CEA-LETI[53]	λ_c = 5.2 µm and 4.6 µm	p-i-n junction; e-APD; doping in p layer:3 × 10^{16} cm⁻³; doping of n⁺ region: 1 × 10^{18} cm⁻³; epitaxial grown by MBE and LPE	384 × 288 MWIR APD FPA; 15µm pitch size, operating temp~ 80 K	Highest Gain achieved ~ 13,000 at -13.8; F value less than 1.4; operability~ 99.7%; Image demonstrated by HgCdTe based FPA with 1 µs integration time and gain of 30.
EPIR and Univ. of Illinois[37,51]	λ_c= 4.9 µm	p⁺-n⁻- n⁺ APD, Epilayer grown on Si substrate grown by MBE;	400 µm × 400 µm diode area;	R_oA~ 3 x 10^6; Gain ~ 1250 at reverse bias -10 V; F= 1 to 1.2, operating temp. = 77 K;
BAE system[38]	λ_c= 3.54 µm, 4.06 µm and 4.23 µm	planar n-on-p e-APD; epitaxial grown by LPE; doping in p-layer is 2 × 10^{16} cm⁻³	4×4 array with unit cell 250×250 µm²;	BW = 500 MHz; Gain measured up to 700; Q.E. >90%; gain normalized dark current < 1pA; gain was measured at different temperature and various diode area
Raytheon vision system[8,45]	λ_c=1.55 µm	Epitaxial wafers grown by both LPE and MBE techniques	16×2, 32×1, 10×10 for linear array; diameter of diodes having 50 to 300 µm;	Band width = 100 MHz Gain >20 for single APD; gain >10 for linear arrays; NEP < 2nW; high fill factor (>80%); low crosstalk (2%); I_{dark} = <10nA; rise time < 10ns
EPIR Technol.[63]	λ_c = 4.6 µm	HDVIP diode HDVIP e-APD ; p-around-n front side-illuminated n⁺/n⁻/p geometry, epilayer grown by MBE	640×480 array, 12 µm pitch	Electrical signal response~ 15 mV/ and NEDT~ 24-27 mK; operability> 99%; operating temp at 77 K and 120 K, value of noise: 0.381 to 0.41
DRS Infrared Technol.[30,49,61]	λ_c = 4.3 / 5.1 µm	HDVIP e-APD; p-around-n front side- illuminated n⁺/n⁻/p geometry, doping in n⁻ region: 4-5 ×10^{14} cm⁻³.	128 × 128 array; Pixel pitch: 40 µm;	Gain: >1000 with value of F~ 1.3; gain normalized dark current : < 1 nA/cm²; measureable input noise equivalent photon (NEPh) ~ 0.4 photons; BW~ 100 MHz
SELEX Galileo (U.K.) and European Southern Lab. (Germay)[55-56]	λ_c = 2.64 µm (SWIR)	Cylindrical p-around-n loophole HDVIP diode	320 × 256 array, Pixel pitch: 24 µm	Gain ~ 7.5 at -7.2 V; dark current ~ negligible with integration time of 40 ms; 2D and 3D images demonstrated using 1.5 µm laser pulse.

concentration 2×10^{16} cm⁻³ are used for fabrication of planar n⁺/v/p⁺ HgCdTe e-APD. Back side illuminated APD detector arrays are fabricated in 320×256 matrix at 30 µm × 30 µm pitch using photolithography, mesa isolation of diodes, passivation, metallisation, and further indium bump deposition. Two layer passivation of ZnS/CdTe is deposited after mesa isolation of diodes. 1000 Å CdTe passivation layer capped by 2500Å of ZnS is deposited after wet etching of the front surface of

HgCdTe epilayers. Inter-diffusion process is used for optimum interface charge density at the CdTe passivation-HgCdTe interface. ZnS/YF$_3$ double layer anti-reflection coating is deposited after polishing of CdZnTe substrate. The device is fabricated by boron-ion implantation with a dose of 5×10^{14} ions cm^{-2} at 180 keV followed by 5×10^{14} ions cm^{-2} at 80 keV to form junction on p-HgCdTe epilayers. A three step process of ion implantation, post implantation annealing in inert environment and second implantation is required to tailor the doping profile in the form of n$^+$/v/p$^+$ configuration. Implantation and post implantation annealing are used to form a v-region with optimum width and low N$_D$-N$_A$ doping by redistributing the donors. Metal layers are deposited for the formation of p- and n-contacts. Differential Hall measurements are revealed a thinner n$^+$ layer layer on top having N$_D$-N$_A$ ~ 1×10^{19} cm^{-3}, ~1.1 µm v-region with (N$_D$-N$_A$) ~ 4×10^{14} cm^{-3}, and p$^+$ layer with N$_A$-N$_D$ ~ 2×10^{16} cm^{-3}.

The devices are exposed to the 300 K background during the dark current and the dark plus photocurrent versus voltage were measurement at 80 K. Figure 5 shows the dark current and dark plus photo current as a function of reverse bias. Therefore, gain is determined from the I-V measurements under illumination condition. The avalanche gain M is calculated by normalizing the photo current for MWIR APD at 80 K and is given as[4,44].

$$M = \frac{I_{illu\,min\,ated}(V) - I_{dark}(V)}{I_{illu\,min\,ated}(V=0) - I_{dark}(V=0)} \qquad (8)$$

The multiplication gain of n$^+$-v-p$^+$ typical diode under reverse bias is shown in the Figure 6. High gain ~ 800 has been achieved for moderate reverse bias of -8 V. Exponential gain-voltage curve and low excess noise factor even at multiplication gain up to 800 at -8 V is a promising result.
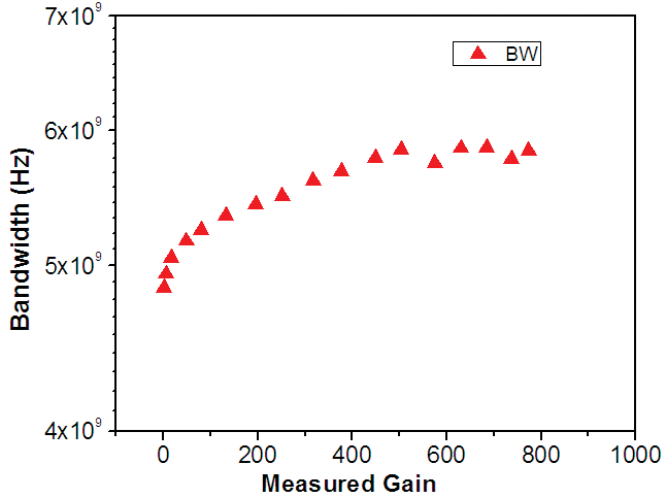

Figure 6. Calculated bandwidth as a function of measured gain. Bandwidth shows independent behavior with gain.

Figure 6 shows the estimated bandwidth versus gain for 4.8 µm cutoff e-APD. Band width is independent of gain in the fabricated MWIR e-APD. The BW is limited by the transit time in the figure. At gain up to 800, the bandwidth > 6 GHz is sufficient for application in high speed free-space optical communication systems. High gain at low bias with GBW~ THz has been achieved with a low excess noise in HgCdTe MWIR
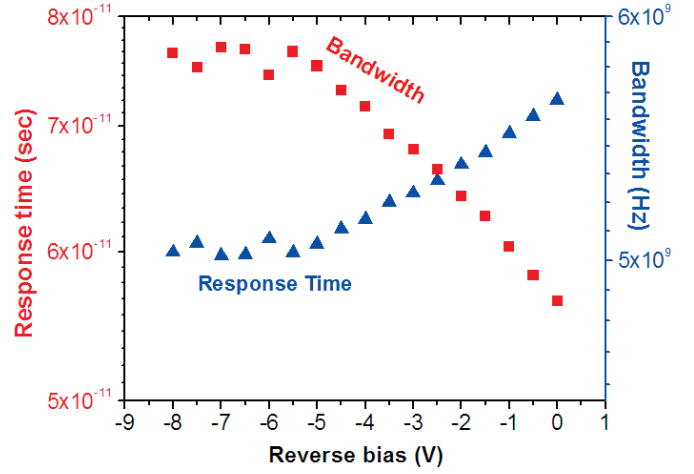

Figure 7. Estimation of response time and bandwidth versus applied reverse bias for n$^+$-v-p$^+$ HgCdTe e-APD.

e- APDs[11,47]. The simulated response time is shown in the Fig. 7. The response time is calculated using one dimensional model taking into account the gain, drift velocity of the electron, position of infrared light injection in the junction and RC time constant. Estimated response time is determined in the range of 0.5 ps corresponds to gain bandwidth product of THz regime.

3.4 Applications

APD provides a combination of fast response time, high sensitivity and high quantum efficiency. These are widely used in high speed and space applications. HgCdTe APD is an attractive choice for many IR applications such as LIDAR/LADAR, defence, night vision, optical communications & atmospheric studies[9-11,45-46]. HgCdTe based SWIR APDs can be used as sensor in the LADAR system or 3-D imaging applications[40, 47-60].

CEA-LETI has been involved in the development of HgCdTe based e-APD focal plane array for Passive (thermal imaging) and active (2D/3D flash LADAR imaging) imaging since last a few years. They have developed a new prototype of flash LADAR dedicated 320 × 256 MWIR APD FPA with 30 µm pixel pitch operating at 80 K. The 2D and 3D active images have been demonstrated using the LADAR system. This demonstration is big achievement in the direction of space application using APD based 3D flash LADAR receiver.

Fast response time is required in laser range finder applications. For accurate determination of target range, the FPA must allow high speed counting by amplification of the returned laser pulse with a good signal to noise ratio. HgCdTe APDs is also suitable candidate in high-speed quantum computing applications.

4. CONCLUSIONS

We have measured the gain of 800 at - 8 V bias and BW~ 6 GHz at 77 K in the fabricated HgCdTe based MWIR e-APD device. The estimated BW is independent of gain and hence can provide faster response time for thermal imaging application at long range condition. HgCdTe based e-APDs offer high gain (~ 10^4) and BW (~ THz) with low excess noise at low reverse bias. HgCdTe based e-APD devices provide low

dark current, higher quantum efficiency and high operability in a large array format. These characteristics are beneficial for thermal imaging application in low flux conditions. APDs can operate with lower light levels and shorter laser pulses thus making more eye safe in the laser range finder applications.

REFERENCES

1. Sze, S.M. Semiconductor devices physics and technology. Ed 2nd. John Wiley and Sons, Inc., 2002. pp.117-120.

2. McIntyre, R.J. A new look at impact ionisation-part I: a theory of gain, noise, breakdown probability, and frequency response. *IEEE Trans. Electron Dev.*, 1999, **46**(8), 1623-1631.
   doi: 10.1109/16.777150

3. Singh, A.; Srivastav, V. & Pal, R. HgCdTe avalanche photodiodes: a review. *Optics Laser technol.*, 2011, **43**, 1358-1370.
   doi: 10.1016/j.optlastec.2011.03.009

4. Singh, A.; Shukla, A.K. & Pal, R. High performance of mid wave infrared HgCdTe e-avalanche photodiode detector. *IEEE Electron Dev. Lett.*, 2015, **36**(4), 360.
   doi: 10.1109/LED.2015.2400571

5. Sudharsanan, R.; Yuan, P.; Boisvert, J.; MacDonald, P. & Isshiki, T. Single photon counting geiger mode InGaAs(P)/InP avalanche photodiode arrays for 3D imaging. *Proc SPIE*, 2008, **6950**, 69500N.
   doi: 10.1117/12.778278

6. Itzler, M.A.; Entwistle, M.; Owens, M.; Patel, K. & Jiang, X. Geiger-mode avalanche photodiode focal plane arrays for three-dimensional imaging LADAR. *Proc SPIE*, 2010, **7808**, 78080C.
   doi: 10.1117/12.861600

7. Huntington, A.S.; Compton, M. A. & Williams, G.M. Linear mode single photon APD detectors. *Proc. SPIE*, 2007, **6771**, 67710Q.
   doi: 10.1117/12.751925

8. Jack, M.; Asbrock, J.; Anderson, C.; Bailey, S.; Chapman, G.; Gordan, E.; Herning, P.; Kalisher, M.; Kosai, K.; Liquori, V.; Randall, V.; Rosbeck, J.; Sen, S. & Wetzel, P. Advances in linear and area HgCdTe APD arrays for eyesafe LADAR sensors. *Proc. SPIE,* 2001, **4454**, 198-211.
   doi: 10.1117/12.448175

9. Asbrock, J.; Bailey, S.; Baley, D.; Boisvert, J.; Chapman, G.; Crawford, G. Ultra-high sensitive APD based 3 D LADAR sensors: Linear mode photon counting LADAR camera for the ultra-sensitive detector program. *Proc, SPIE, 2008,* **6940**, 69402O.
   doi: 10.1117/12.783940

10. Campbell, J. C.; Demiguel, S.; Ma, F.; Beck, A.; Guo, X.; Wang, S. Recent advances in avalanche photodiodes. *IEEE J. Sel. Top. Quant.,* 2004, **10**(4), 777-787.
    doi: 10.1109/JSTQE.2004.833971

11. Rothman, J.; Perrais, G.; Destefanis, G.; Baylet, J.; Castelein, P. & Chamonal, J.P. High performance characteristics in pin MW HgCdTe e-APDs. *Proc. SPIE*, 2007, **6542**, 654219:1- 10.
    doi: 10.1117/12.723465

12. Abautret, J.; Perez, J.P.; Evirgen, A.; Martinez, F.; Christol, P. Electrical modeling of InSb PiN photodiode for avalanche operation. *J. Appl. Phys.*, 2013, **113**, 183716.
    doi: 10.1063/1.4804956

13. Demiguel, S. Theoretical analysis and comparison of SWIR active imaging detectors. *Proc, SPIE,* 2009, **7298**, 729836:1-10.
    doi: 10.1117/12.817926

14. Ruden, P. P. & Krishnankutty, S. A solar blind, hybrid III-nitride/silicon ultraviolet avalanche photodiode. *IEEE Trans. Electron Dev.,* 1999, **46**(12), 2348-2350.
    doi: 10.1109/16.808080

15. Ulmer, M.P. A review of UV detectors for astrophysics: past, present, and future. *Proc. SPIE*, 2009, **7222**, 722210.
    doi: 10.1117/12.810039

16. Sood, A.K.; Richwine, R.A. & Puri, Y.R. Design considerations using APD detectors for high-resolution UV imaging applications. *Proc SPIE*, 2009, **7419**, 74190V.
    doi: 10.1117/12.829899

17. Lin, J. C.; Su, Y. K.; Chang, S. J.; Lan, W. H.; Huang, K. C.; Chen, W. R.; Huang, C. Y.; Lai, W.C.; Lin, W.J. & Cheng, Y.C. High responsivity of GaN p-i-n photodiode by using low-temperature interlayer. *Appl. Phys. Lett.,* 2007, **91**, 173502:1-3.
    doi: 10.1063/1.2800813

18. Yan, F.; Zhao, J.H. & Olsen, G.H. Demonstration of the first 4H-SiC avalanche photodiodes. Solid state electron, 2000, **44**, 341-46.
    doi: 10.1016/S0038-1101(99)00240-3

19. Pauchard, A.; Besse, P.-A.; Bartek, M.; Wolffenbuttel, R. F. & Popovic, R. S. Ultraviolet–selective avalanche photodiode. *Sensor Actuator,* 2000, **82**,128-134.
    doi: 10.1016/S0924-4247(99)00326-X

20. Marshall, A.R.J.; David, J.P.R. & Tan, C.H. Impact ionisation in InAs electron avalanche photodiode. *IEEE Trans Electron Device*, 2010, **57**(10), 2631-38.
    doi: 10.1109/TED.2010.2058330

21. Maurya, P. K.; Agarwal, H.; Singh, A. & Chakrabarti, P. InAs/InAsSb avalanche photodiode (APD) for applications in long-wavelength infrared region. *Opto-electron. Lett.,* 2008, **4**(5), 342-346.
    doi: 10.1007/s11801-008-8068-5

22. David, J.P.R. & Tan, C.H. Material consideration for avalanche photodiodes. *IEEE J. Selected Quantum Electronics*, 2008, **14**(4), 998-1009.
    doi: 10.1109/JSTQE.2008.918313

23. Rouvie, A.; Carpentier, D.; Lagay, N.; Decobert, J.; Pommereau, F. & Achouche, M. High gain and band width product over 140 GHz planar junction AlInAs avalanche photodiodes. *IEEE Photon Technol Letter*, 2008, **20**(6), 455-57.
    doi: 10.1109/LPT.2008.918229

24. Ramirez, D.A.; Shao, J.; Hayat, M.M. & Krishna, S. Midwave infrared quantum dot avalanche photodiode. *Appl Phys Lett*, 2010, **97**, 221106.
    doi: 10.1063/1.3520519

25. Leveque, G.; Nasser, M.; Bertho, D.; Orsal, B. & Alabedra, R. Ionisation energies in Hg$_{1-x}$Cd$_x$Te avalanche

photodiode. *Semicond. Sci. Tech.,* 1993, **8**, 1317-1323. doi: 10.1088/0268-1242/8/7/021

26. Beck, J. D.; Wan, C. F.; Kinch, M. A. & Robinson, J. E. MWIR HgCdTe avalanche photodiodes. *Proc. SPIE* , 2001, **4454**,188-197.
    doi: 10.1117/12.448174

27. Kinch, M. A.; Beck, J. D.; Wan, C. F.; Ma, F. & Campbell, J. HgCdTe electron avalanche photodiodes. *J. Electron Mater.,* 2004, **33**(6), 630-639.
    doi: 10.1007/s11664-004-0058-1

28. Lecoy, G. P.; Orsal, B. & Alabedra, R. Impact ionisation resonance and auger recombination in $Hg_{1-x}Cd_xTe$ (0.6 £ x£ 0.7). *IEEE J. Quantum Elect.,* 1987, **23**(7), 1145-1154. doi: 10.1109/JQE.1987.1073494

29. Ma, F.; Li, X.; Campbell, J. C.; Beck, J. D.; Wan, C. F. & Kinch, M. A. Monte carlo simulations of $Hg_{0.7}Cd_{0.3}Te$ avalanche photodiodes and resonance phenomenon in the multiplication noise. *Appl. Phys. Lett.,* 2003, **83**(4), 785-787.
    doi: 10.1063/1.1596727

30. Beck, J.; Wan, C.; Kinch, M.; Robinson, J.; Mitra, P.; Scritchfield, R.; Ma, F. & Campbell, J. The HgCdTe electron avalanche photodiode. *J. Electron Mater.,* 2006, **35**(6),1166-1173.
    doi: 10.1007/s11664-006-0237-3

31. Hall, R. S.; Gordan, N.T.; Giess, J.; Hails, J. E.; Graham, A.; Herbert, D.C. & Hall, D.J. Photo multiplication with low excess noise factor in MWIR to optical fiber compatible wavelengths in cooled HgCdTe mesa diodes. *Proc. SPIE,* 2005, **5783**, 412-423.
    doi: 10.1117/12.603386

32. Shin, S.H.; Pasko, J.G.; Law, H.D. & Cheung, D.T. 1.22 µm HgCdTe/CdTe avalanche photodiodes. *Appl. Phys. Lett.,* 1982, **40**(11), 965-967.
    doi: 10.1063/1.92969

33. Alabedra, R.; Orsal, B.; Lecoy, G.; Pichard, G.; Meslage, J. & Fragnon, P. An $Hg_{0.3}Cd_{0.7}Te$ avalanche photodiode for optical-fiber transmission systems at l=1.3mm. *IEEE Trans. Electron Dev.,*1985, **32**(7),1302-1306.
    doi: 10.1109/T-ED.1985.22115

34. Orsal, B.; Alabedra, R.; Valenza, M.; Lecoy, G. P.; Meslage, J. & Boisrobert, J. $Hg_{0.4}Cd_{0.6}Te$ 1.55-mm avalanche photodiode noise analysis in the vicinity of resonant impact ionisation connected with the spin-orbit split-off band. *IEEE Trans. Electron Dev.,* 1988, **35**(1), 101-107.
    doi: 10.1109/16.2424

35. Elliott, C.T.; Gordon, N.T.; Hall, R.S. & Crimes, G. Reverse breakdown in long wavelength lateral collection $Hg_{1-x}Cd_xTe$ diodes. *J. Vac. Sci. Technol. A,* 1990, **8**(2), 1251-1253.
    doi: 10.1116/1.576954

36. Vaidyanathan, G.; Joshi, A.; Xue, S.; Hanyaloglu, B.; Thomas, M.; Zandian, M.; Edwall, D.; Williams, G.; Blackwell, J.; Tennant, W. & Hughes, G. High Performance Ladar Focal Plane Arrays for 3D Range Imaging. *IEEE Aerospace Conference Proc.3,* 2004, **1776**.

37. Mallick, S.; Banerjee, K.; Velicu, S.; Grien, C.; Ghosh,

S. & Zhao, J. Avalanche mechanism in p+-n⁻-n+ and p+-n mid-wavelength infrared $Hg_{1-x}Cd_xTe$ diodes on Si substrates. *J. Electron. Mater*., 2008, **37**(9), 1488-1496. doi: 10.1007/s11664-008-0518-0

38. Reine, M. B.; Marciniec, J. W.; Wong, K. K.; Parodos, T.; Mullarkey, J. D.; Lamarre, P.A. ; Tobin, S. P.; Minich, R. W.; Gustavsen, K.A.; Compton, M. & Williams, G.M. Characterisation of HgCdTe MWIR back illuminated electron-initiated avalanche photodiodes. *J. Electron. Mater.,* 2008, **37**(9), 1376-1386.
    doi: 10.1007/s11664-008-0420-9

39. Perrais, G.; Derelle, S.; Mollard, L.; Chamonal, J. P.; Destefanis, G.; Vincent, G.; Bernhardt, S. & Rothman, J. Study of the transit-time limitations of the impulse response in mid-wave infrared HgCdTe avalanche photodiode. *J. Electron Mater.,* 2009, **38**(8), 1790-1799. doi: 10.1007/s11664-009-0802-7

40. Hunter, A.T. Avalanche photodiodes for detection of eye-safe laser pulses. *Proc. SPIE,* 1999, **3629**, 250.
    doi: 10.1117/12.344561

41. Shockley, W. Problems related to p-n junction in Silicon. *Solid State Electron,* 1961, **2**(1), 35-67.
    doi: 10.1016/0038-1101(61)90054-5

42. Rothman, J.; Mollard, L.; Gout, S.; Bonnefond, L. & Wlassow, J. History dependent impact ionisation theory applied to HgCdTe e-APDs. *J. Electron Mater*, 2011, **40**(8), 1757-68. doi: 10.1007/s11664-011-1679-9

43. Capper, P. & Garland, J. Mercury cadmium telluride growth, properties and application. U.K., John Wiley and Sons Ltd., pp.493-511, 2011.

44. Perrais, G.; Gravrand, O.; Baylet, J.; Destefanis, G. & Rothman, J. Gain and dark current characteristics of planar HgCdTe avalanche photodiodes. *J. Electron. Mater.,* 2007, **36**(8), 963-970.
    doi: 10.1007/s11664-007-0147-z

45. Jack, M.; Asbrock, J.; Bailey, S.; Baley, D.; Chapman, G.; Crawford, G.; Drafahl, B.; Herrin, E.; Kvaas, R. & McKeag, W. MBE based HgCdTe APDs and 3D LADAR sensors. *Proc. SPIE,* 2007, **6542***,* 65421A: 1-11.
    doi: 10.1117/12.724347

46. Guellec, F.; Tchagaspanian, M.; Borniol, E.; Castelein, P.; Perez, A. & Rothman, J. Advanced pixel design for infrared 3D LADAR imaging. *Proc. SPIE,* 2008, **6940**, 69402M:1-10. doi: 10.1117/12.779284

47. Perrais, G.; Rothman, J.; Destefanis, G. & Chamonal, J. P. Impulse response time measurements in $Hg_{0.7}Cd_{0.3}Te$ MWIR avalanche photodiodes. *J. Electron Mater.,* 2008, **37**(9), 1261-1273. doi: 10.1007/s11664-008-0459-7

48. Singh, A.; Shukla, A. K. & Pal, R. HgCdTe e-avalanche photodiode detector arrays. AIP Advances, 2015, **5**, 087172. doi: 10.1063/1.4929773

49. Beck, J.; Scritchfield, R.; Sullivan, B.; Teherani, J.; Wan, C. F.; Kinch, M.; Ohlson, M.; Skokan, M.; Wood, L.; Mitra, P.; Goodwin, M. & Robinson, J. Performance and modeling of the MWIR HgCdTe electron avalanche photodiode. *J. Electron Mater.,* 2009, **38**(8),1579-1592. doi: 10.1007/s11664-009-0684-8

50. Rothman, J.; Baier, N.; Ballet, P.; Mollard, L.; Fournier,

M.; Gout, J.S. & Chamonal, J. P. High-operating-temperature HgCdTe avalanche photodiodes. *J. Electron. Mater.,* 2009, **38**(8),1707-1716.
doi: 10.1007/s11664-009-0823-2

51. Ghosh, S.; Mallick, S.; Banerjee, K.; Grein, C.; Velicu, S.; Zhao, J.; Silversmith, D.; Rodriguez, J. B.; Plis, E. & Krishna, S. Low-noise mid-wavelength infrared avalanche photodiodes. *J. Electron. Mater*., 2008, **37**(12), 1764-1769.
doi: 10.1007/s11664-008-0542-0

52. Williams, G.M.; Compton, M.A. & Huntington, A.S. High-speed photon counting with linear-mode APD receivers. *Proc. SPIE,* 2009, **7320**, 732012.
doi: 10.1117/12.817862

53. Kerlain, A.; Bonnouvrier, G.; Rubaldo, L.; Decaens, G. & Reibel, Y. Performance of mid-wave infrared HgCdTe e-avalanche photodiodes. *J. Electron. Mater.*, 2012, **41**(10), 2943-48.
doi: 10.1007/s11664-012-2087-5

54. Mahlein, K.M.; Bauer, A.; Bitterlich, H.; Bruder, M.; Gassmann, K.U.; Haiml, M.; Hanna, S.; Nothaft, H.P.; Wollrab, R. & Ziegler, J. Next generation IR sensor technology for space applications at AIM. *Proc. SPIE,* 2008, **7106***,* 71061J.
doi: 10.1117/12.800307

55. Finger, G.; Baker, I.; Dorn, R.; Eschbaumer, S.; Ives, D. & Mehrgan, L. Development of high speed low noise IR HgCdTe avalanche photodiode arrays for adaptive optics and interferometry. *Proc. SPIE*, 2010, **7742**, 77421K.
doi: 10.1117/12.857316

56. Ashcroft, A. & Baker, I. Developments in HgCdTe avalanche photodiode technology and applications. *Proc. SPIE*, 2010, **7660**, 76603C.
doi: 10.1117/12.850133

57. Borniol, Eric de; Castelein, P.; Guellec, F.; Rothman, J. & Vojetta, G. A 320x256 HgCdTe avalanche photodiode focal plane array for passive and active 2D and 3D imaging. *Proc. SPIE*, 2011, **8012**, 801232.
doi: 10.1117/12.884466

58. Aqariden, F.; Elsworth, J.; Zhao, J.; Grein, C.H. & Sivananthan, S. MBE HgCdTe for HDVIP devices: Horizontal integration in the US HgCdTe FPA industry. *J. Electron. Mater.*, 2012, **41**(10), 2700-06.
doi: 10.1007/s11664-012-2189-0

59. Rothman, J.; Mollard, L.; Bosson, S.; Vojetta, G.; Foubert, K. & Gatti, S. Short wave infrared HgCdTe avalanche photodiodes. *J. Electron Mater*, 2012, **41**(10), 2928-36.
doi: 10.1007/s11664-012-1970-4

60. Gravrand, O.; Mollard, L.; Boulade, O.; Moreau, V.; Sanson, E. & Destefanis, G. Ultralow dark current HgCdTe FPAs in the SWIR range at CEA and sofradir. *J. Electron Mater*, 2012, **41**(10), 2686-2693.
doi: 10.1007/s11664-012-2181-8

61. Beck, J.; Welch, T.; Mitra, P.; Reiff, K.; Sun, X. & Abshire, J. A highly sensitive multi-element HgCdTe e-APD detector for IPDA Lidar applications. *J. Electon. Mater*., 2014, **43**(8), 2970-2977.
doi: 10.1007/s11664-014-3164-8

62. Rothman, J.; Foubert, K.; Lasfargues, G. & Largeron, C. Response time measurements in short-wave infrared HgCdTe e-APDs. *J. Electron. Mater*., 2014, **43**(8), 2947-2954.
doi: 10.1007/s11664-014-3155-9

63. Aqariden, F.; Elsworth, J.; Zhao, J.; Grein, C.H. & Sivananthan, S. MBE HgCdTe for HDVIP devices: Horizontal integration in the US HgCdTe FPA industry. *J. Electron. Mater.*, 2012, **41**(10), 2700-06.
doi: 10.1007/s11664-012-2189-0

ACKNOWLEDGEMENT

CONTRIBUTORS

Mr Anand Singh received the MSc from University of Rajasthan, Jaipur, in 2001. He is currently pursuing his PhD from Indian Institute of Technology, Delhi, India. Currently working as a Scientist at Solid State Physics Laboratory, New Delhi. He is actively working in the field of II-VI and III-V based infrared detector. His research interests include : Design, fabrication and characterisation of infrared photodetector, with emphasis on Avalanche Photodiodes.

Dr Ravinder Pal received MSc, MTech and PhD from Indian Institute of Technology, Delhi, India. Currently working as a Scientist 'G' and heading Infrared Technology Development Division at Solid State Physics Laboratory, Delhi. He also served as a Guest Faculty at Microelectronics Research Group at the University of Western Australia (UWA), Australia during 2000-2001. His interests include : Development of III-V and II-VI based infrared focal plane array (IRFPA).